We are IntechOpen, the world's leading publisher of Open Access books Built by scientists, for scientists

6,900
Open access books available

185,000
International authors and editors

200M
Downloads

Our authors are among the

154
Countries delivered to

TOP 1%
most cited scientists

12.2%
Contributors from top 500 universities

WEB OF SCIENCE™

Selection of our books indexed in the Book Citation Index in Web of Science™ Core Collection (BKCI)

Interested in publishing with us?
Contact book.department@intechopen.com

Numbers displayed above are based on latest data collected.
For more information visit www.intechopen.com

Chapter 6

Application of a Hydrodynamic and Water Quality Model for Inland Surface Water Systems

Lubo Liu

Additional information is available at the end of the chapter

http://dx.doi.org/10.5772/intechopen.74914

Abstract

This chapter introduces basic concepts, properties, and principles of different processes in inland surface water and analytical methodologies. The fundamentals of surface water hydrodynamics, including water properties, hydrodynamic processes, Cartesian coordinate-based governing equations, and boundary and initial conditions were reviewed. The fate and transport of contaminants in surface water were introduced. Based on aforementioned theory and principles, two hydrodynamic-water quality models were developed for studying a lake and a river, respectively. A stratified 3D model was used to investigate the circulation and *E. coli* transport in the nearshore region of Lake Michigan. The modeling results show that stratified phenomenon exists in the near region, and a 3D model is necessary even though a previous 2D model works well for the shallow water environment. A 2D depth-averaged water quality model was developed to estimate the fate and transport of four contaminants in the San Joaquin River of California. The modeling results indicate that it took 20 days for these contaminants to transport from the upstream to the downstream in the research domain. These models can be effectively used for inland surface water restoration and management.

Keywords: inland, surface water, hydrodynamics, water quality, numerical model

1. Introduction to surface water systems

Inland surface water systems such as rivers, streams, creeks, lakes, reservoirs, and wetlands play a hugely important role in our drinking water supply, agricultural irrigation, industrial utilization, recreational activities, and other public uses. Our everyday lives depend on the availability and quality of surface water. Surface water is in motion in response to natural forces, climatic effects, and human activities, all of which have a significant impact on its

IntechOpen

© 2018 The Author(s). Licensee IntechOpen. This chapter is distributed under the terms of the Creative Commons Attribution License (http://creativecommons.org/licenses/by/3.0), which permits unrestricted use, distribution, and reproduction in any medium, provided the original work is properly cited. CC BY

quality. Although surface water systems are governed by many different factors, this chapter focuses primarily on two of the most influential aspects: hydrodynamics and water quality. Water's hydrodynamic characteristics include its flow velocity, water depth, and water surface elevation, while water quality is assessed in terms of its physical (temperature, color, odor, sediments, etc.), chemical (dissolved oxygen, salinity, organic matter and heavy metal content, nutrients, etc.), and biological characteristics (bacteria, viruses, protozoans, etc.). The interactions between the processes related to these characteristics are inevitably fairly complex; water system administrators must therefore seek to develop a good understanding of the dominant factors and processes that affect the water quality of each of the local water resources they are responsible for if they are to make correct or optimized management decisions.

Water quality is represented by the levels of a series of water quality parameters such as water temperature, dissolved oxygen, level of pathogens, and the concentrations of different chemicals, all of which may vary both temporally and spatially. In addition to the inactivation of contaminants, the levels and distribution of contaminants are governed by several dynamic processes, including diffusion, dispersion, and advection. These processes are closely linked to the water's flow characteristics, the influents and effluents entering and leaving the body of water, wind stress, the Coriolis effect (which must be taken into account in large bodies of water such as the Great Lakes), and stratified temperature, among other factors. In turn, the fate and transport of contaminants may influence flow, for example, sediment transport may change flow density. In addition to these common mechanisms shared by all surface water bodies, each will have its own unique characteristics. Therefore, to better understand how a particular surface water system functions, essential knowledge of its hydrodynamic and water quality related processes must be supplemented by information regarding its specific characteristics.

The methods typically used to study the surface water systems include theoretical analyses, mathematical modeling, laboratory experiments, and field observations. Experiments and observations are the most reliable ways to acquire real information for a specific system that will provide a good basis for analysis and modeling. However, for a complex surface water body, the observed or measured data are usually far from sufficient to reflect or predict a complete picture of the real scenario. Furthermore, the available data are not necessarily totally reliable, and low quality data with high errors may lead researchers to build a false or misleading idea of what is actually happening. Therefore, mathematical modeling coupled with observations for verification and calibration is essential in such cases. Hydrodynamic and water quality models have been widely developed and used for the investigations of rivers [1–4], lakes or reservoirs [5–11], estuaries [12, 13], and coastal waters [14, 15] on various aspects. These models have been effective tools for explaining, simulating, and forecasting the complex processes in water environment.

This chapter focuses on the fundamental concepts and principles of surface water analysis, and the application of a model that combines hydrodynamics and water quality. The goals are to help develop a better understanding of the different hydrodynamic processes involved to facilitate decision making in real surface water systems. After a discussion on the fundamentals of surface water hydrodynamics (Section 2), contaminant fate and transport in surface water and a water quality model will be discussed. This chapter concludes with a discussion of two case studies of very different surface water systems, the southern part of Lake Michigan and the upper reaches

of the San Joaquin River in California, to illustrate how these theoretical predictions compare to the hydrodynamic and water quality properties observed in real bodies of water.

2. Fundamentals of surface water hydrodynamics

Hydrodynamics deals with the motion of water and the forces acting on water. Hydrodynamic studies focus on investigating the mechanisms driving flow by quantifying the key physical processes in water. The results obtained provide invaluable information on the movement and transport of contaminants, which serves as the basis for all research into water quality. The information needed to develop a hydrodynamic model includes a comprehensive set of governing equations that describe the physical processes involved and the associated initial and boundary conditions required to numerically solve the equations, and the various parameters that must be input to run the model.

2.1. Water properties and hydrodynamic processes

In hydrodynamics, the main property parameters of water are its density/specific weight and its viscosity, both of which have a significant impact on the solutions to the governing equations. The density of water can vary depending on the temperature, concentration of the suspended solids, and salinity. The influence of these factors on water density has been formulated as follows [16]:

$$\rho = \rho_T + \Delta\rho_S + \Delta\rho_C \tag{1}$$

where ρ_T is the density of pure water as a function of temperature T [17, 18], $\Delta\rho_S$ is the change in density due to salinity S, and $\Delta\rho_C$ is the change in density due to total suspended sediments [19].

Viscosity represents the internal friction of water and is very important for hydrodynamic processes. The kinematic viscosity (m^2/s) of a river can be approximated as a function of temperature T (°C) [20].

$$\upsilon = \left(1.785 - 0.0584T + 0.00116T^2 - 0.0000102T^3\right) \times 10^{-6} \tag{2}$$

Here, hydrodynamic processes refer to water motion, circulation, mixing phenomena; the corresponding processes involving the materials suspended in the water include advection, dispersion and mixing. The results combine to form a hydrodynamic model that generally includes flow field, water depth and water surface elevation, salinity, temperature, and sediment concentration. Some of this information, for example, which related to temperature, salinity, and/or sediment, may also be utilized in water quality models.

2.2. Cartesian coordinate-based governing equations

The governing equations for both water flow and the transport of contaminants are based on the conservation laws of mass, momentum, and energy. Hydrodynamic models include two main types of governing equations: continuity equation for the mass balance of water in the

Model dimensions	Characteristics	Applications
Zero	Completely mixed, no flow, spatially uniform	Estimation of ponds, lakes, tanks with no or low flow
One	Shallow narrow flow, well mixed, spatial variation in transverse and vertical directions neglected	Long creeks, rivers, streams, narrow channels
Two (horizontal)	Shallow wide flow, well mixed, spatial variations in vertical direction neglected	Wide open lakes and estuaries (weakly stratified), ponds, wide shallow river reaches
Two (vertical)	Deep narrow flow, spatial variation in lateral direction neglected	Narrow and deep lakes, reservoirs, river reaches (strongly stratified)
Three	Deep, stratified flow, significant variation in vertical direction, all three directions considered	Deep large lakes, reservoirs, coastal regions, estuaries

Table 1. Examples of different dimensional models and their applications.

flow and momentum equation that indicates the relationship between the driving forces and water acceleration of motion, which is Newton's second law. The forces acting on a water body include gravity, viscous force, and pressure as well as other external forces such as wind and the Coriolis force. The momentum equation in most hydrodynamic models is a simplification and/or modification of the Navier-Stokes equation. Most natural surface water systems are characterized as "shallow water," where the horizontal scale is far greater than the water depth. The hydrostatic assumption, which assumes that the hydrostatic balance in the vertical plane and the vertical acceleration can be neglected, also applies to shallow water. Technically, all surface water systems are three-dimensional scenarios, and a fully 3D model would thus provide the most complete description of their flow features, but the resulting model would be far too complex for the governing equations to be solved. Under most circumstances, it is reasonable to use a 1D, 2D, or quasi-3D model as this provides sufficient accuracy to solve nearly all practical problems. Based on the representation and spatial scale of water body and application purposes, a number of different dimensional models have been developed by researchers. Examples of these models and their applications are listed in **Table 1**. Their governing equations for continuity and momentum are described as follows [20] (2.2.1), [16, 20] (2.2.3), [21] (2.2.2), [23] (2.2.4).

2.2.1. 1D equations

2.2.1.1. Continuity equation

$$\frac{\partial A}{\partial t} + \frac{\partial (Au)}{\partial x} = 0 \tag{3}$$

2.2.1.2. Momentum equation

$$\frac{\partial (Au)}{\partial t} + \frac{\partial \left(Au^2\right)}{\partial x} + gA\left[\frac{\partial (a+h)}{\partial x}\right] - \frac{1}{\rho}\frac{\partial}{\partial x}\left(\varepsilon_{xx} A \frac{\partial u}{\partial x}\right) - \frac{1}{\rho}(B\tau_{sx} - \lambda\tau_{bx}) = 0 \tag{4}$$

where A is the cross sectional area, u is the flow velocity averaged over the cross section, a is the elevation of channel bottom, h is the water depth, ε_{xx} is the horizontal eddy coefficient, B is the channel width at the water surface, λ is the wetted perimeter of the cross section, τ_{sx} is the wind stress acting on water surface, and τ_{bx} is the frictional stress on bottom and bank surface [20].

2.2.2. Depth-averaged 2D equations

2.2.2.1. Continuity equation

$$\frac{\partial h}{\partial t} + u\frac{\partial (h)}{\partial x} + v\frac{\partial (h)}{\partial y} + h\left(\frac{\partial u}{\partial x} + \frac{\partial v}{\partial y}\right) = 0 \tag{5}$$

2.2.2.2. Momentum equations

$$\begin{aligned} &h\frac{\partial u}{\partial t} + hu\frac{\partial u}{\partial x} + hv\frac{\partial u}{\partial y} - fvh = \frac{1}{\rho}\left[\frac{\partial}{\partial x}\left(\overline{\varepsilon}_{xx}h\frac{\partial u}{\partial x}\right) + \frac{\partial}{\partial y}\left(\overline{\varepsilon}_{xy}h\frac{\partial u}{\partial y}\right)\right] \\ &-gh\left(\frac{\partial a}{\partial x} + \frac{\partial h}{\partial x}\right) - \frac{ugn^2\sqrt{(u^2+v^2)}}{h^{4/3}} + \zeta W^2\cos\psi \end{aligned} \tag{6}$$

$$\begin{aligned} &h\frac{\partial v}{\partial t} + hu\frac{\partial v}{\partial x} + hv\frac{\partial v}{\partial y} - fuh = \frac{1}{\rho}\left[\frac{\partial}{\partial x}\left(\overline{\varepsilon}_{yx}h\frac{\partial v}{\partial x}\right) + \frac{\partial}{\partial y}\left(\overline{\varepsilon}_{yy}h\frac{\partial v}{\partial y}\right)\right] \\ &-gh\left(\frac{\partial a}{\partial y} + \frac{\partial h}{\partial y}\right) - \frac{vgn^2\sqrt{(u^2+v^2)}}{h^{4/3}} + \zeta W^2\sin\psi \end{aligned} \tag{7}$$

where u, v are the depth-averaged velocities in the x, y directions, respectively, W is the wind velocity, ψ is the wind direction, ζ is the empirical wind coefficient; f is the Coriolis parameter, g is the acceleration due to gravity, n is the Manning's roughness coefficient, and $\overline{\varepsilon}$ is the depth-averaged eddy viscosity. Horizontal mixing is described using the Smagorinsky eddy parameterization:

$$\overline{\varepsilon} = 2A_m = \alpha A\left[\left(\frac{\partial u}{\partial x}\right)^2 + \left(\frac{\partial v}{\partial y}\right)^2 + \frac{1}{2}\left(\frac{\partial u}{\partial y} + \frac{\partial v}{\partial x}\right)^2\right]^{\frac{1}{2}} \tag{8}$$

where α is a constant in the range 0.01–0.5 [22] and A_m is the area of the current element based on the finite element scheme [21].

2.2.3. Lateral-averaged 2D equations

2.2.3.1. Continuity equation

$$\frac{\partial (Bu)}{\partial x} + \frac{\partial (Bw)}{\partial z} = 0 \tag{9}$$

where u is the lateral averaged velocity in the x direction, w is the lateral averaged velocity in the z direction, and B is the water width.

2.2.3.2. Momentum equation

$$\frac{\partial(Bu)}{\partial t}+\frac{\partial\left(Bu^2\right)}{\partial x}+\frac{\partial(uwB)}{\partial z}+gB\frac{\partial(z_s)}{\partial x}-\frac{\partial}{\partial x}\left(BA_H\frac{\partial u}{\partial x}\right)-\frac{\partial}{\partial x}\left(BA_v\frac{\partial u}{\partial z}\right)-\tau_x=0 \tag{10}$$

where A_H is the horizontal eddy viscosity, A_v is the vertical turbulent mixing coefficient, and z_s is the water surface elevation. For gradually varying flows, the z-direction momentum equation can be neglected due to the insignificant effects of inertia, diffusion, and dispersion in the vertical direction [16, 20].

2.2.4. 3D stratified flow equations

2.2.4.1. Continuity equation

$$\frac{\partial u}{\partial x}+\frac{\partial y}{\partial y}+\frac{\partial w}{\partial z}=0 \tag{11}$$

Based on the hydrostatic assumption Eq. (12), vertical momentum equations can be eliminated from 3D governing equations.

$$\frac{\partial p}{\partial z}+\rho g=0 \tag{12}$$

For the purposes of this analysis, a water system is divided into a series of horizontal layers that interact with each other. The topography of a real 3D environment is generally nonuniform, and the bathymetry may spatially differ over a wide range. To avoid any problems due to the nonuniform water depth, it is necessary to transform the system to a constant geometric structure with uniform resolution. Based on the Sigma method [16, 23, 24], a transformation scheme was developed as follows:

$$\begin{aligned} x' &= x \\ y' &= y \\ z' &= a+\frac{(z-a)(b-a)}{h} \end{aligned} \tag{13}$$

where x',y',z' are the transformed coordinates, p is the water pressure, g is the acceleration due to gravity, ρ is the water density, z is the vertical coordinate, a is the bottom elevation, and b is the fixed vertical location to which the water surface will be transformed. Thus, the continuity equation and momentum equations along the horizontal direction are as follows [23]:

$$\begin{aligned} &\frac{\partial h}{\partial t}+\int_a^b\left[\frac{\partial u}{\partial x}-\frac{(b-a)}{h}\frac{\partial u}{\partial z}T_x+\frac{\partial v}{\partial y}-\frac{(b-a)}{h}\frac{\partial v}{\partial z}T_y\right]dz+u_s\frac{\partial(a+h)}{\partial x}-u_b\frac{\partial a}{\partial x} \\ &+v_s\frac{\partial(a+h)}{\partial y}-v_b\frac{\partial a}{\partial y}=0 \end{aligned} \tag{14}$$

$$\begin{aligned}
&\rho h\frac{\partial u}{\partial t}+\rho hu\frac{\partial u}{\partial x}+\rho hv\frac{\partial u}{\partial y}+\rho\frac{\partial u}{\partial z}\left[(b-a)\left(w-uT_x-vT_y\right)-(z-a)\frac{\partial h}{\partial t}\right]\\
&-(b-a)\frac{\partial}{\partial x}\left(\varepsilon_{xx}\frac{h}{(b-a)}\frac{\partial u}{\partial x}\right)-(b-a)\frac{\partial}{\partial y}\left(\varepsilon_{xy}\frac{h}{(b-a)}\frac{\partial u}{\partial y}\right)\\
&-(b-a)\frac{\partial}{\partial z}\left(\varepsilon_{xz}\frac{\partial u}{\partial z}\right)+\rho_s gh\frac{\partial a}{\partial x}+\rho_s gh\frac{\partial h}{\partial x}+g_x h-\Gamma_x=0
\end{aligned} \tag{15}$$

$$\begin{aligned}
&\rho h\frac{\partial v}{\partial t}+\rho hu\frac{\partial v}{\partial x}+\rho hv\frac{\partial v}{\partial y}+\rho\frac{\partial v}{\partial z}\left[(b-a)\left(w-uT_x-vT_y\right)-(z-a)\frac{\partial h}{\partial t}\right]\\
&-(b-a)\frac{\partial}{\partial x}\left(\varepsilon_{yx}\frac{h}{(b-a)}\frac{\partial v}{\partial x}\right)-(b-a)\frac{\partial}{\partial y}\left(\varepsilon_{yy}\frac{h}{(b-a)}\frac{\partial v}{\partial y}\right)\\
&-(b-a)\frac{\partial}{\partial z}\left(\varepsilon_{yz}\frac{\partial v}{\partial z}\right)+\rho_s gh\frac{\partial a}{\partial y}+\rho_s gh\frac{\partial h}{\partial h}+g_y h-\Gamma_y=0
\end{aligned} \tag{16}$$

where u, v, w are the velocities in the x, y, z direction, respectively, ε_{ij} is the turbulent eddy coefficient ($i, j = x, y, z$), Γ_i is the external tractions on the water body, and ρ_s is the density at the water surface. Subscripts s and b denote surface and bottom, respectively.

Eddy viscosity can be determined using a number of different methods, but the Mellor Yamada formulation [25] and the Smagorinsky [22] method are the among most widely used methods for the horizontal and vertical eddy viscosity, respectively.

2.3. Boundary and initial conditions

To numerically solve these governing equations, boundary conditions (and initial conditions for transition problems) must be specified for all external surfaces of the water body. Boundaries of a surface water system consist of the top water surface and the bottom and side surfaces. Accordingly, the water surface elevation, the velocities at the bottom and side surfaces, and the flux (if sediment and salinity are to be considered) at all boundaries must be specified.

2.3.1. The free water surface

There is zero pressure on the water surface and no leakage across the water surface.

$$w_s = \frac{dh}{dt} \tag{17}$$

where w_s is the vertical velocity at the water surface. There may also be some external surface traction, such as wind stress, acting on the water surface.

2.3.2. The bottom surface

Two types of boundary conditions are applied to the bottom surface [23], which will be either a no leakage boundary or a no slip boundary ($u_b = v_b = w_b = 0$) condition.

2.3.3. The side surface

The side surface refers to the shoreline of the water body or a defined boundary of the model such as the entrance or exit of a river reach. The shoreline conditions are zero normal velocity, that is, no leakage across the boundary surface. Information on the water surface elevation, velocities, or flow rate need to be specified for the defined boundaries, but combinations of different conditions should be avoided on the same boundary.

2.3.4. Other boundary conditions

In addition to the required boundary conditions mentioned earlier, some frictional stresses Γ_i in the governing equations may act on the surfaces of water body so the corresponding conditions should be added to the model. Common stresses include wind stress (Γ_{WX} and Γ_{WY}) and frictional stress (Γ_{BX} and Γ_{BY}).

2.3.5. Initial conditions

A dynamic model requires a set of initial values to be input in order to begin to solve the governing equations. The model needs a "best guess" set of conditions for all the nodes in the mesh at the beginning of the iterative process; a bad initial guess that is far from the real conditions will adversely affect the convergence, slowing down the process immensely. A commonly used strategy is to have the whole water body at rest with a constant water surface elevation (WSE) when t = 0. The real initial scenario generally emerges after running the simulation for a period from this initial state.

2.4. Parameters and data for the hydrodynamic model

Many different types of data are needed as input or to determine the controlling parameters when running a hydrodynamic model. The data used as direct input include the geographic coordinates of the shoreline, bathymetry, flow rate, water surface elevation, meteorological data such as wind speed and direction, radiation intensity, air pressure, precipitation and the evaporation rate, among others. In addition to the input data, data on the flow rate, velocities, water depth, and water surface elevation at other locations than the boundaries are also needed to calibrate the model to determine hard to measure parameters such as the roughness of the bottom and the horizontal momentum diffusion coefficient [16], and to confirm that the model accurately reflects the real scenario. The modeling results are compared to the data measured either in the laboratory or in the field for the model calibration and verification.

3. Water quality model

Water quality, which includes its physical, chemical, biological, and other characteristics, is predominantly controlled by the hydrodynamic processes and the various mechanisms governing the fate and transport of contaminants. Once a contaminant enters a water system, its concentration is determined by its chemical and biological reactions and hydrodynamic transport processes, including advection, dispersion, and vertical mixing. Water quality models

are widely used to reflect these processes. Some examples of water quality model applications include the simulation and prediction of water temperature, dissolved oxygen (DO), biochemical oxygen demand (BOD), the nitrogen cycle (including levels of organic nitrogen, ammonia, nitrite and nitrate), the phosphorous cycle (including levels of organic phosphorous and phosphates), algae growth and decay, cohesive/noncohesive suspended sediment, salinity, heavy metals, and pathogens, among others [27]. Depending on the results for advection, dispersion, and turbulent mixing obtained from the hydrodynamic model, water quality models may also incorporate the sources/sinks, chemical and biological reactions of contaminants.

3.1. Governing equations for contaminant fate and transport

The governing equations for contaminant fate and transport are as follows [16, 21, 23]:

3.1.1. 1D equation

$$\frac{\partial(A_s C)}{\partial t} + \frac{\partial(AuC)}{\partial x} - \frac{\partial}{\partial x}\left(D_x A \frac{\partial C}{\partial x}\right) - kA_s C \pm G = 0 \tag{18}$$

3.1.2. 2D depth-averaged equation

$$\begin{aligned} &\frac{\partial(hC)}{\partial t} + u\frac{\partial(hC)}{\partial x} + v\frac{\partial(hC)}{\partial y} - \frac{\partial}{\partial x}\left(D_x h\frac{\partial C}{\partial x} + D_{xy} h\frac{\partial C}{\partial y}\right) \\ &-\frac{\partial}{\partial y}\left(D_{xy} h\frac{\partial C}{\partial y} + D_y h\frac{\partial C}{\partial y}\right) - khC \pm G = 0 \end{aligned} \tag{19}$$

3.1.3. 2D laterally averaged equation

$$\begin{aligned} &\frac{\partial(BC)}{\partial t} + u\frac{\partial(uBC)}{\partial x} + v\frac{\partial(wBC)}{\partial z} - \frac{\partial}{\partial x}\left(BD_x\frac{\partial C}{\partial x}\right) - \frac{\partial}{\partial x}\left(BD_z\frac{\partial C}{\partial z}\right) \\ &-khC \pm G = 0 \end{aligned} \tag{20}$$

3.1.4. 3D stratified equation

$$\begin{aligned} &h\frac{\partial C}{\partial t} + h\frac{\partial(uC)}{\partial x} + h\frac{\partial(vC)}{\partial y} + (b-a)\frac{\partial(wC)}{\partial z} - (b-a)T_x\frac{\partial(uC)}{\partial z} \\ &-(b-a)T_y\frac{\partial(vC)}{\partial z} - h\frac{\partial}{\partial x}\left(D_x\frac{\partial C}{\partial x} + D_{xy}\frac{\partial C}{\partial y}\right) + h\frac{\partial}{\partial x}\left[\frac{(b-a)}{h}\left(D_x T_x + D_{xy}T_y\right)\frac{\partial C}{\partial z}\right] \\ &+(b-a)T_x\frac{\partial}{\partial z}\left(D_x\frac{\partial C}{\partial x} + D_{xy}\frac{\partial C}{\partial y}\right) - (b-a)T_x\frac{\partial}{\partial z}\left[\frac{(b-a)}{h}\left(D_x T_x + D_{xy}T_y\right)\frac{\partial C}{\partial z}\right] \\ &-h\frac{\partial}{\partial y}\left(D_{xy}\frac{\partial C}{\partial x} + D_y\frac{\partial C}{\partial y}\right) + h\frac{\partial}{\partial y}\left[\frac{(b-a)}{h}\left(D_{xy}T_x + D_y T_y\right)\frac{\partial C}{\partial z}\right] \\ &+(b-a)T_y\frac{\partial}{\partial z}\left[\frac{(b-a)}{h}\left(D_{xy}T_x + D_y T_y\right)\frac{\partial C}{\partial z}\right] \\ &-(b-a)\frac{\partial}{\partial z}\left[D_z\frac{(b-a)}{h}\frac{\partial C}{\partial z}\right] - khC \pm G - (b-a)\frac{\partial(v_s C)}{\partial z} = 0 \end{aligned} \tag{21}$$

where C is the concentration of the contaminant or temperature, A is the cross-sectional area, A_s is the storage cross-sectional area, D_i is the turbulent diffusion coefficient in the i direction, G is a general term representing sources or sinks, and k is the first order decay or reproductive rate coefficient [23]. These equations represent the first order case; other reaction rates (such as zero order or second order) are described using different expressions for the source term. The terminology used for the other variables is same as that used in Section 2.

3.2. Boundary and initial conditions

Contaminants may be released into a water system via one of two modes: constant release or pulsed release. For both, the initial condition is $C(x, t = 0) = C_0$, where C_0 is the initial concentration that can be assigned as a constant such as the background concentration. The boundary condition for the free surface, bottom and side surfaces is the no flux condition, $\frac{\partial C}{\partial n} = 0$, where n represents the coordinates in the direction normal to the boundary. Other observed concentrations are assigned to the inflow and outflow boundaries.

3.3. Parameters and data for the water quality model

For a water quality model, numerous parameters and data are needed as input. Initial values for these parameters are obtained from the literature, measured directly, or determined via model calibration. The modeling results for various values of the parameter are then compared against the observed data, and the value that achieves the best match is selected for further modeling runs.

Water quality models are fairly complex due to the multiple interrelationships among the many processes controlling the fate and transport of contaminants. Many of these processes can only be described using empirical formulations, which need adequate data for verification and calibration. Data quantity and quality are thus keys for developing and applying a water quality model. In the remainder of this chapter, finite element model RMA10 is used as the hydrodynamic model and RMA11 as the water quality model in the discussion [23].

4. Case studies

Two case studies, the application of a hydrodynamic model in a lake and a water quality model in a river, are presented in this section to show how the respective models are applied for real world surface water systems.

4.1. Case study 1: Southern Lake Michigan

4.1.1. Background

Water quality in the nearshore region of southern Lake Michigan had a problem with contamination by fecal bacteria from various sources. For Great Lakes beaches, fecal pollution attracted a great deal of attention from both beach managers and the public due to its potential

risk to human health, triggering many beach closures and advisories every year with a consequent significant loss to local economies along the shoreline. Predictive modeling has been suggested as an effective approach to enhancing measurements of water quality both temporally and spatially, thus reducing the damage caused by improving the beach management. This case study was therefore conducted to develop a nearshore transport model for fecal pollution in Lake Michigan. The resulting model can be used to inform beach goers promptly in order to protect them from any potential exposure to waterborne pathogens and to help develop a better understanding of the key processes and factors influencing the fate and transport of fecal pollution in the nearshore reaches of the lake. As the indicators of fecal bacteria, Escherichia coli (EC) and enterococci (ENT) were used to evaluate the water quality at a recreational beach. In such environments, modeling nearshore, wind-driven circulation and the transport of EC and ENT are particularly challenging due to the interactions with complex lake-wide circulation. Originally, a 2D depth-averaged model was developed to simulate the entire lake with finer meshes close to the shoreline to emphasize the nearshore region [21]. The modeling results show that the current in nearshore region flew predominately along the shoreline direction and the cross-shoreline flow was fairly weak. Therefore, within an acceptable error tolerance range, the entire lake can be simplified as a narrow channel along the shoreline to significantly save computation efforts for nearshore process investigations. With this simplification, current flows only in clockwise or anticlockwise direction along the shoreline, and the exchanging process of mass and momentum in cross-shoreline direction only occur within the channel [26]. Later investigation indicates that the current in vertical direction sometimes cannot be neglected in such lake environment, and thus, a stratified 3D model may be necessary to explain the hydrodynamic and transport processes along the water depth. In this case study, a new 3D model for the domain model was developed based on the aforementioned channelized 2D model. Some 3D modeling results are reported in the following sections.

4.1.2. Investigation domain and model mesh

This case study focused on the nearshore regions along approximately 100 km of the shoreline of southern Lake Michigan. Based on the channelization simplification [26], the computational domain included a 5-km wide channel throughout the entire Lake Michigan shoreline (**Figure 1**). To fairly delineate the complex shoreline, a finite element model with a 3D nonuniform mesh was used. The mesh was gradually refined from a resolution of approximately 1–2 km at the locations far from the research domain to 100 m in the research area. Four streams are the primary tributaries discharging into southern Lake Michigan: Trail Creek (TC) at the Michigan City Harbor (USGS 04095380), Kintzele Ditch (KD) nearby Michigan City, Burns Ditch at Portage, IN (BD, USGS 04095090), and Indiana Harbor Canal (IHC) at East Chicago. As KD and TC both discharge combined sewer flows (CSOs), these are the most significant sources of EC and ENT so Mt. Baldy beach, which is located between the two, was chosen as the nearshore beach for this investigation (**Figure 1**).

4.1.3. Data collection

Major factors considered in the model included the bathymetry, the shape of the lake shoreline, wind stress, hydrological flows from the tributaries, and water temperature. Bathymetric data

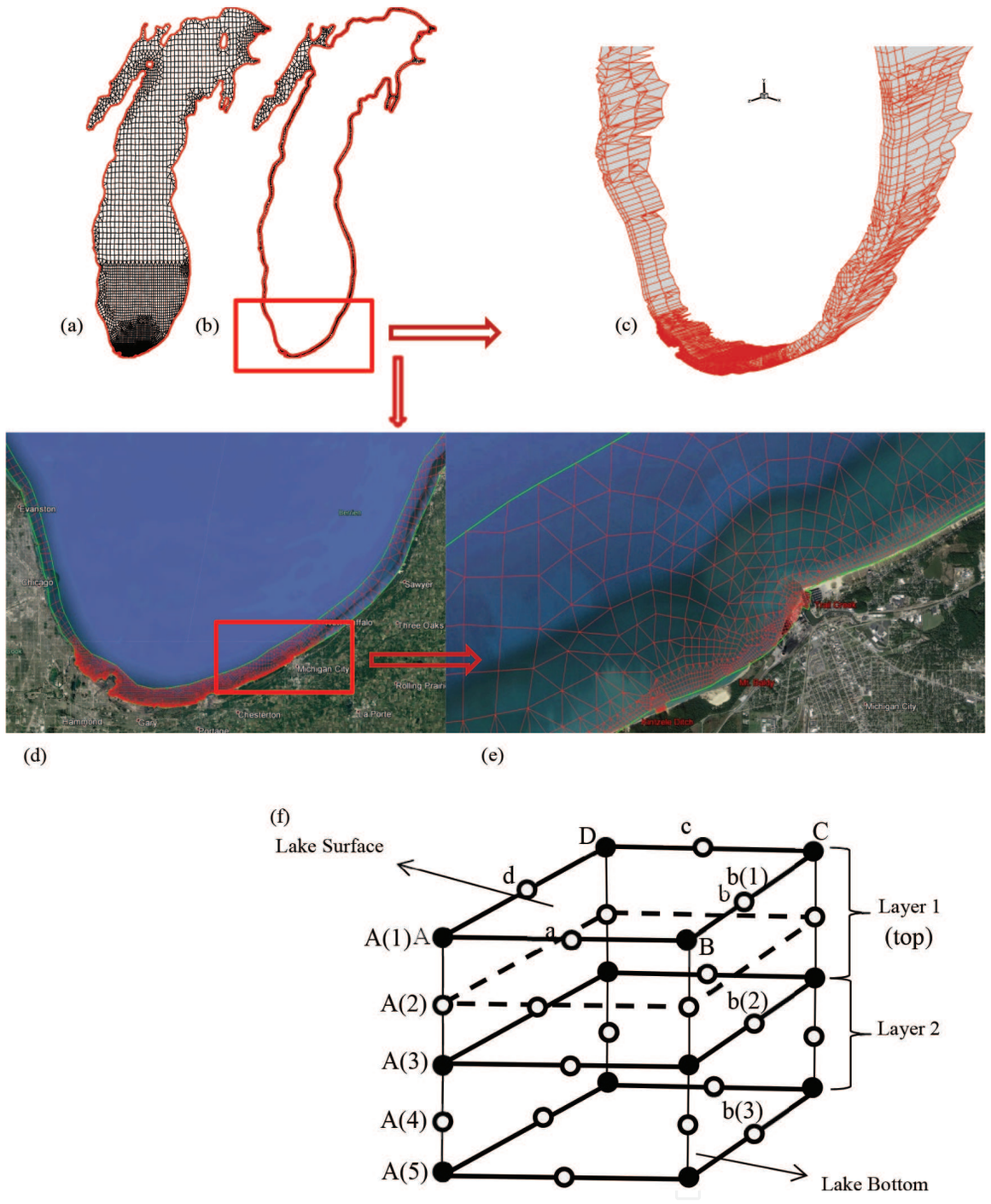

Figure 1. (a) Whole lake model mesh (2D), (b) channelized mesh (2D), (c) channelized mesh (3D), (d) Google Earth satellite image with the channelized mesh, (e) enlarged research domain with mesh, and (f) scheme of node distribution in quadratic a 3D element mesh.

with a resolution of 3 arc-seconds were obtained from the NOAA's National Geophysical Data Center. As inputs of the model, hourly meteorological data, including wind speed and direction, air temperature, dew point temperature, air pressure, and sunlight insolation were obtained from six stations run by NOAA's National Climatic Data Center and two buoys belonging to NOAA's National Data Buoy Center (NDBC). Data on current velocity and WSE were also collected from several stations for model calibration.

4.1.4. Hydrodynamic and water quality model

4.1.4.1. Model description

Although a 2D depth-averaged model based on the finite element model RMA10 [21, 26] can well describe the wind-driven circulation at the particular location in Lake Michigan during the specific period, the transport phenomenon along the water depth is fairly significant for other contaminants at other locations [27]. Therefore, a stratified 3D hydrodynamic and water quality model was developed to address the vertical current and transport. The model was employed to simulate current velocity, water depth, water surface elevation, water temperature, and EC. The model principles and setup, including the governing equations, boundary conditions, and initial conditions, were those described earlier in Sections 2 and 3. The governing equations were thus Eqs. (11)–(16) for the hydrodynamic model and Eq. (21) for the water quality model. A constant value of 2.0 m^2/s was used for both the eddy viscosity and the turbulent diffusion coefficient in the nearshore region. The water body was evenly divided into three layers, and thus, there are totally either five nodes (for the corner points in a finite element) or three nodes (for the mid-points in a finite element) at each location throughout the water depth. **Figure 1f** shows the nodes constituting a typical finite element in the 3D mesh. A quadratic finite element consists of corner nodes (solid dots such as A, B, C, and D) and middle nodes (empty dots such as a, b, c, and d). In this two-layer mesh, four and two nodes are placed under each corner and middle node at the water surface, respectively. Therefore, there are totally five (e.g., A(1)–A(5)) or three (e.g., a(1)–a(3)) nodes from the lake surface to the bottom.

4.1.4.2. Initial and boundary conditions

The initial conditions used to model EC were the lake at rest and a background value of 3 CFU/100 mL, based on general observations. The observed water temperatures at the different stations were interpolated into the mesh for the thermal model when t = 0. The boundary conditions for the hydrodynamic model included the no leakage condition across the surface and the bottom, zero pressure and wind stress at the free surface, drag at the bottom surface, and the flow loading from the tributaries. For the water quality model, EC and ENT data were loaded for both TC and KD, and the loading rates were monitored at the stream mouths.

4.1.4.3. Fate and transport of EC and ENT

In addition to determining the hydrodynamic transport processes in the water body, estimating the activation rate of EC and ENT is another key issue in the model. The common factors affecting the fate and transport of EC and ENT include sunlight, nutrient content, salinity, suspended solids, sedimentation, water temperature, pH, and predation. Based on the important inactivation mechanisms reported in the literature, a time-dependent inactivation rate was used, which considered solar insolation, sedimentation, and water temperature, as shown below:

$$\underbrace{k(I,T,v_s)}_{(1)} = \left[f_P\frac{v_s}{H} + k_I I(t)\right]\theta^{(T-20)} = \underbrace{f_P\frac{v_s}{H}\theta^{(T-20)}}_{(2)} + \underbrace{k_I I(t)\theta^{(T-20)}}_{(3)} \tag{22}$$

where $k(I,T,v_s)$ is the overall inactivation rate, k_I is the inactivation rate for light, $I(t)$ is the measured solar insolation, θ is the temperature correction factor (usually 1.07), f_P is the

fraction of pathogens attached to the suspended sediment, v_s is the settling velocity, and H is the water column depth.

4.1.5. Model calibration

The hydrodynamic model was calibrated by adjusting the Manning's roughness coefficient, n after examining the sensitivity of model currents to the horizontal viscosity. The modeling results were compared with Acoustic Doppler Current Profiler (ADCP) data collected at Burns Ditch (July 2–August 14). **Figure 2** shows these comparisons. A constant bed roughness value of 0.1 leading to a minimum root mean square error (RMSE, Eq. (23)) was finally used in the model. The modeling results for the current velocity and WSE were generally consistent with known circulation patterns in southern Lake Michigan.

$$RMSE = \sqrt{\frac{1}{N}\sum_{i=1}^{N}\left[\log_{10}(X_{sim}) - \log_{10}(X_{obs})\right]^2} \tag{23}$$

where X_{sim}, X_{obs} are the simulated results and the observed data, (referring to the concentrations in this case study), respectively.

4.1.6. Results and discussion

In addition to the previous published 2D modeling investigation of the domain, we examined the 3D modeling results. The modeling concentrations of EC and water temperatures at

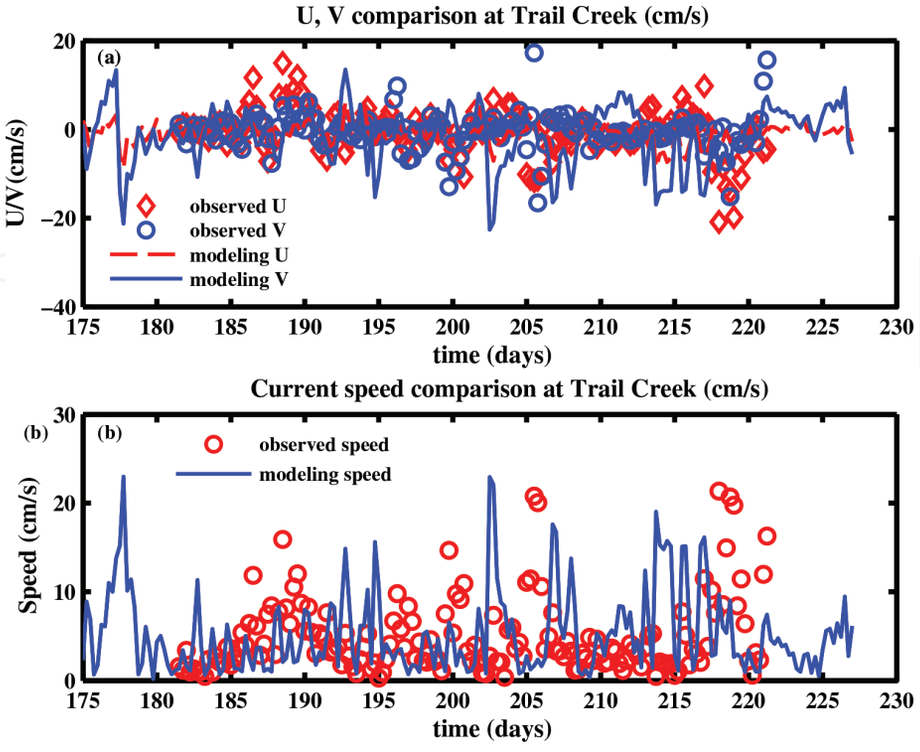

Figure 2. Comparison of (a) velocity component and (b) speed between data and 3D modeling results (lake surface).

http://dx.doi.org/10.5772/intechopen.74914

different depth at the sampling locations were compared with the observed data (**Figures 3** and **4**). Time-dependent inactivation rate based on temperature, sedimentation, and observed solar insolation (Eq. (22)) was used to simulate EC inactivation. The same parameter values as those in the 2D models were used for the 3D model, which include a k_I value of 0.0026 $W^{-1}m^2d^{-1}$, a fraction f_P of 0.1, and a v_s value of 5 m per day. The modeling results at different depth showed a similar pattern of temporal variation, which can reasonably describe the data. Generally, both the speed and the magnitude of velocity components tend to decrease

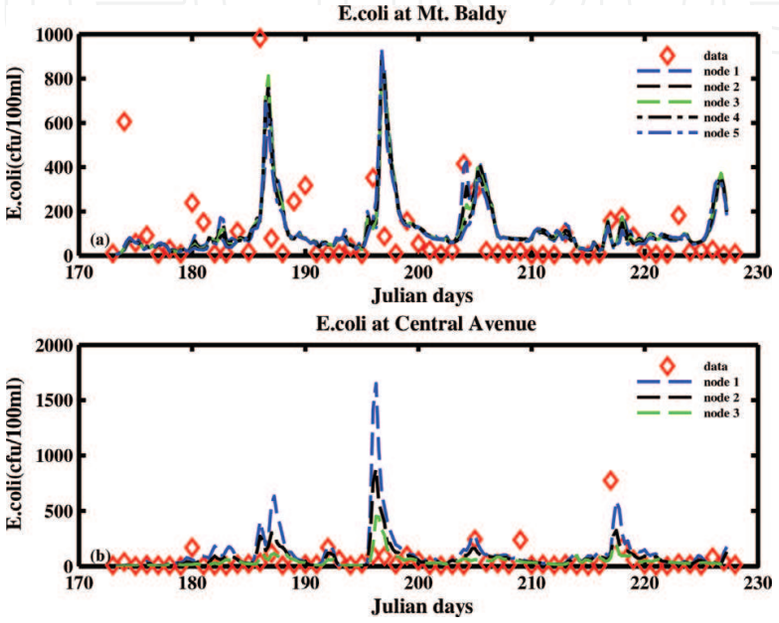

Figure 3. Comparison of *E. coli* between data and 3D modeling results at (a) Mt. Baldy and (b) Central Avenue.

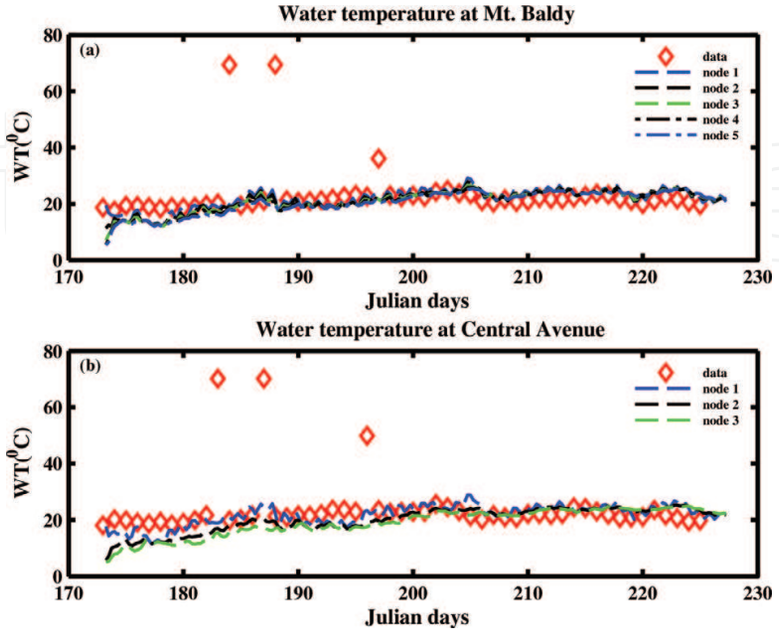

Figure 4. Comparison of temperature between data and 3D modeling results at (a) Mt. Baldy and (b) Central Avenue.

with depth (U, V, W and Speed in **Figures 5**–**7**). The water temperatures at water surface are higher than those below and the lake bottom has the minimum value. **Figures 8** and **9** show the contour of *E. coli* reflecting its transport and fate and water temperature distribution at different time. The model was able to reasonably describe the observed data.

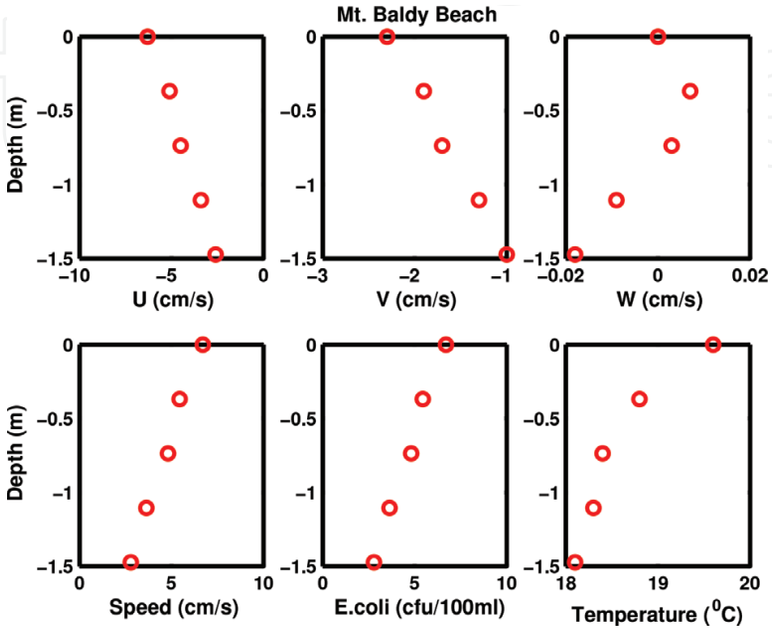

Figure 5. Distribution of calculated parameters along water depth at Julian day 210 at Mt. Baldy Beach.

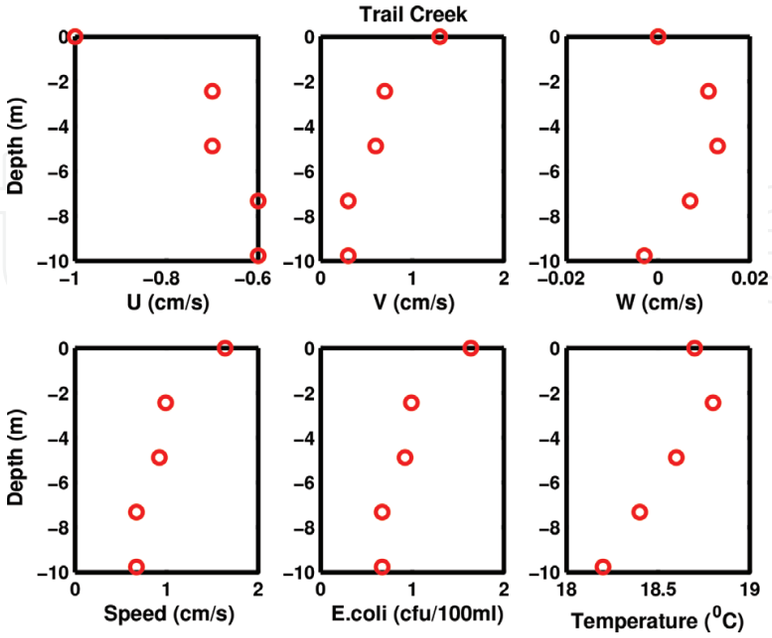

Figure 6. Distribution of calculated parameters along water depth at Julian day 210 at Trail Creek.

http://dx.doi.org/10.5772/intechopen.74914

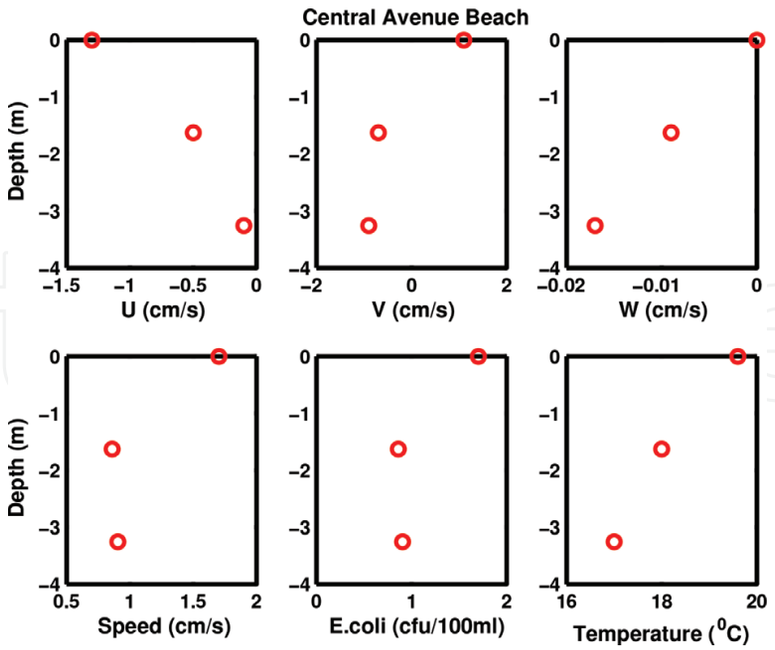

Figure 7. Distribution of calculated parameters along water depth at Julian day 210 at Central Avenue Beach.

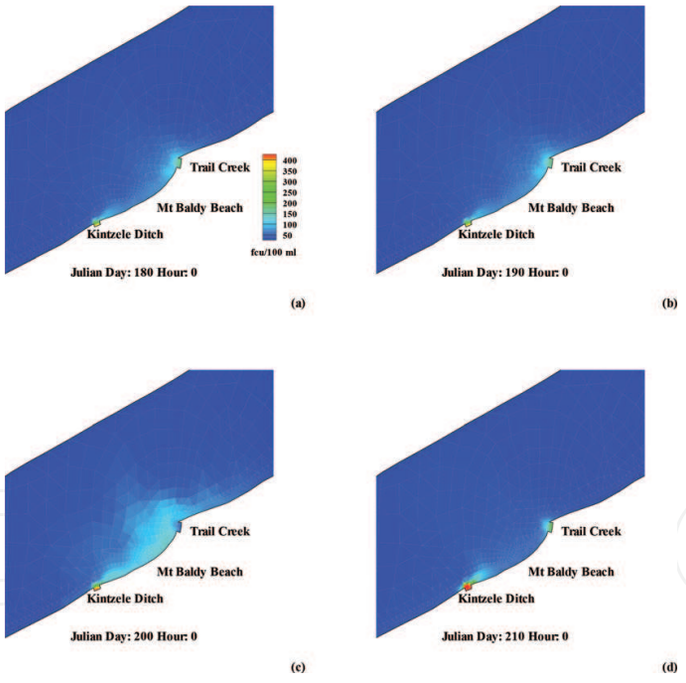

Figure 8. Spatial distribution of *E. coli* at 12:00 am on Julian day: (a) 180, (b) 190, (c) 200, and (d) 210.

4.2. Case study 2: Upper San Joaquin River

4.2.1. Background

The San Joaquin River (SJR) is the second longest river in California, and its watershed within the Central Valley is one of the California's most productive agricultural areas. The river

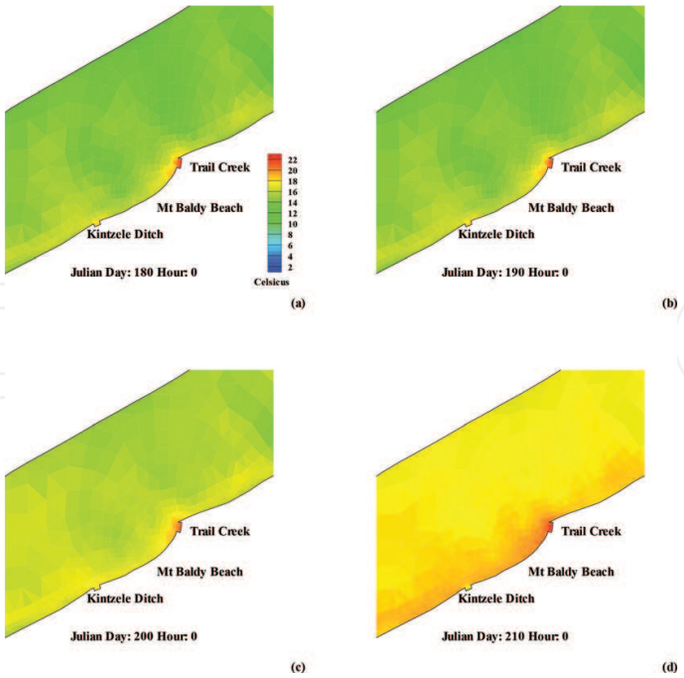

Figure 9. Spatial distribution of water temperature at 12:00 am on Julian day: (a) 180, (b) 190, (c) 200, and (d) 210.

originates mainly from snowmelt and runoff in the high Sierra Nevada, eventually converging with the Sacramento River in the Sacramento-San Joaquin Delta in Northern California. The SJR has experienced considerable low flow over the years, at times ceasing to flow completely. Chinook salmon was historically abundant in the SJR, but their populations have significantly decreased due to the insufficient flow. In order to restore and sustain salmon and other fish populations, the San Joaquin River Restoration Program (SJRRP) was established in 2006 to maintain continuous flow along the entire length of the river and improve its hydrodynamic conditions from Friant Dam to its confluence with the Merced River. Suitable hydrodynamic conditions, including flow velocity and water depth, are crucial for the safe passage of migrating salmon. Due to practical limitations, the flow has been rerouted along several alternative pathways specifically designed and created as part of the river restoration effort, modifying the traditional SJR channels. These alternatives were designed and compared to support the passage of fish by providing adequate hydrodynamic conditions throughout the river reach. The first objective of the research conducted for this case study was to model the stream conditions, including current velocity, depth, and WSE, for three alternatives proposed for the SJRRP given the same hydrologic/hydraulic boundary conditions. This part of hydrodynamic research has been done and published [28]. The second objective was to further investigate how the water quality at the upstream of the SJR affects the downstream. A 2D water depth-integrated water quality model was developed corresponding to the previous hydrodynamic model to simulate and predict the fate and transport of the contaminants in the upper SJR reach. The water quality model will provide a tool for the SJR restoration and management in the future.

4.2.2. Investigation domain and model mesh

The study area covered approximately 90 river kilometers from the SJR monitoring station near Dos Palos (SDP) to the SJR monitoring station at the Fremont Ford Bridge (FFB) near California Highway 140, which is located within the Middle San Joaquin-Lower Chowchilla

watershed. In this case study, alternative 3 was used for the water quality study. The water pathway is: Reach 4A—Eastside Bypass—Mariposa Bypass—Reach 4B2—Reach 5 [28].

The same finite element mesh employed in the hydrodynamic model with resolutions ranging from 0.5 to 50 m was used to delineate the complex boundaries of the SJR.

4.2.3. Data collection

Bathymetric data were collected during 2010 and 2011 by the US Bureau of Reclamation (USBR) using GPS and ADCP at a spatial interval of 6 m. The flow rate and WSE data (from January 1 to September 30 of 2011) used to verify and calibrate the model and as boundary conditions were obtained from the US Geological Survey (USGS), USBR, and the California Department of Water Resources (CADWR). The geographic boundary of the SJR was delineated using coordinates from Google Earth based on the WGS84 global reference system. The data collected from different coordinate systems were all converted and georeferenced using the same coordinate system and reference datum, namely the North American Vertical Datum NAVD 88 and California State Plane, Zone 3, North American horizontal Datum NAD 83. The water quality data are not available at this time.

4.2.4. Model setup

A vertically integrated hydrodynamic model has been employed using the finite element scheme RMA10 to simulate flow velocity, water depth, and WSE. The governing equations were Eqs. (5)–(8). Compared with the first case study, the Coriolis force and wind stress are insignificant and can thus be neglected for this small-scale river reach. For the initial conditions, the river was assumed to be at rest at the beginning and it took a considerable time (10 days) to reach the actual initial conditions. The boundary conditions included the upstream flow rates, the known downstream WSEs, no leakage across the surface and the bottom, a drag stress at the river bottom, no wind stress and zero pressure at the water surface.

4.2.5. Results and discussion

The hydrodynamic model has been calibrated using the 2011 discharge and WSE data set. The Manning roughness coefficient of the river reach was manually adjusted to calibrate the model using the RMSE (Eq. (23)). The optimum value of 0.035 of the coefficient led to the minimum RMSE.

The flow velocity and WSE obtained from the validated and calibrated model were then used to assess the habitat suitability of the SJR reach for the spring Chinook salmon. The detailed model calibration and engineering plan comparisons have been reported by Liu and Ramirez [28]. Due to the lack of observed water quality data, the developed water quality model was used to simulate a virtual scenario as follows: four chemical species, including NH_3, NO_3, Organic N, and Organic P, which are common in the SJR watershed, entered the SJR at the upstream entrance of the river reach (SDP). These contaminants transport to the downstream with water flow and also undergo their own deactivation. **Figure 10** shows the concentrations change with time during a 110-day period. The SDP curve represents the upstream boundary condition. EBM and FFB are the middle station and downstream station, respectively. The

modeling results indicate the similar transport patterns for all species with a time lag between the locations. Generally, it took about 20 days for a contaminant to transport from SDP to FFB for this case. Therefore, the model can also be used to effectively predict the downstream scenario once the upstream condition is known. **Figure 11** shows a spatial distribution of various parameters at some time (the 50th Julian day of 2011 in this example).

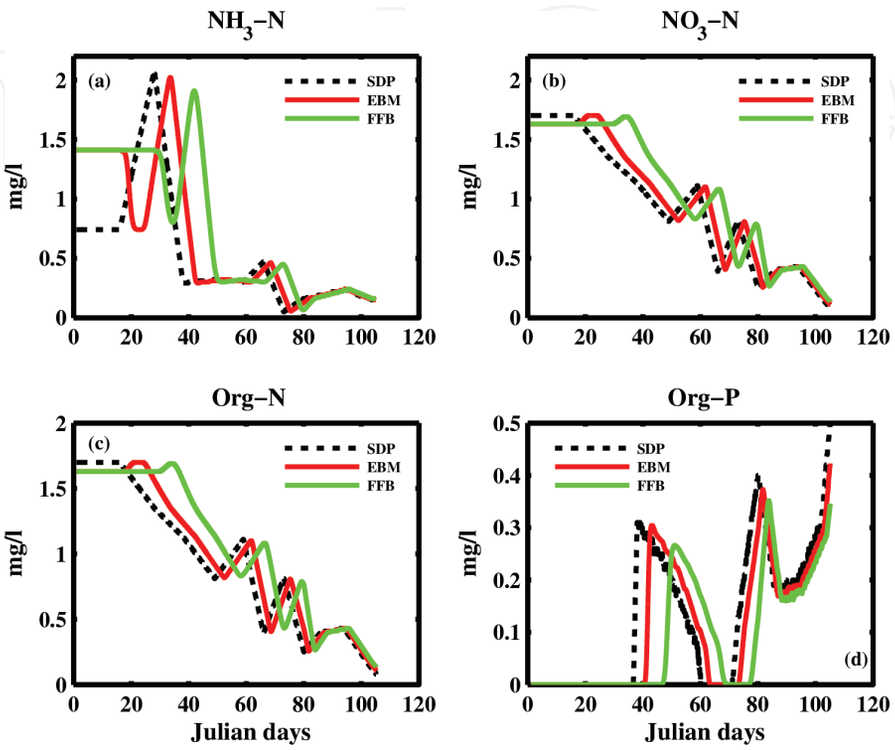

Figure 10. Calculated concentrations of: (a) NH_3-N, (b) NO_3-N, (c) organic N, and (d) organic P.

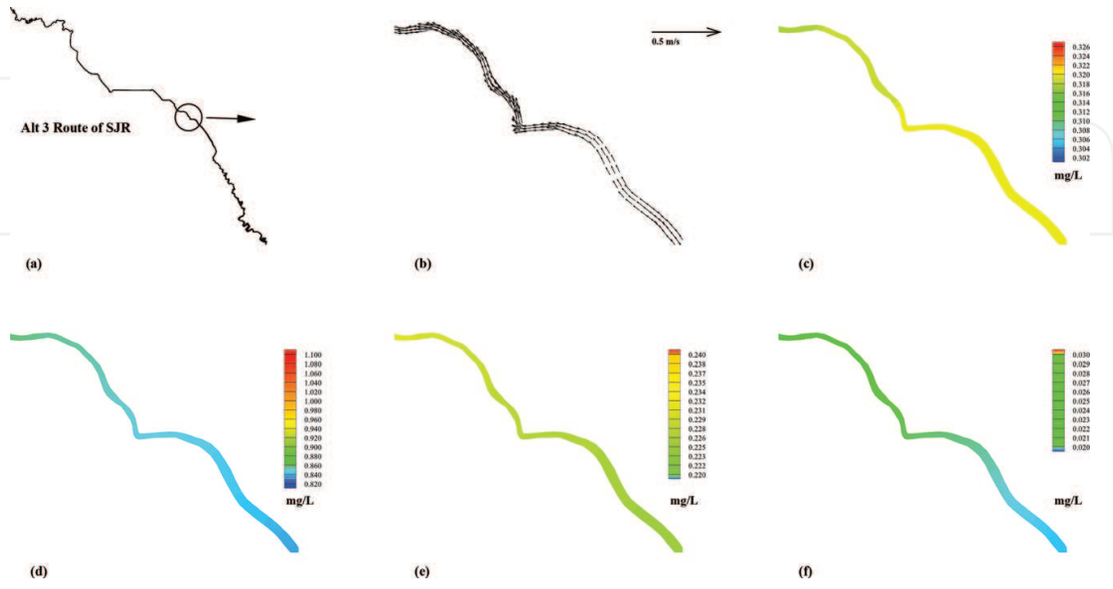

Figure 11. Scheme of (a) Alt3 route of SJR, spatial distributions of (b) velocity vector of Alt 3 of SJR, concentrations (contours) of: (c) NH_3-N, (d) NO_3-N, (e) organic N, and (f) organic P at Julian day 50, 2011.

5. Summary of hydrodynamic-water quality model applications

Based on the fundamental concepts, theories and principles, and the practical examples presented in the two case studies, the steps involved in developing and employing a hydrodynamic-water quality model to simulate or predict a surface water system can be summarized as follows:

1. Determine the modeling domain and identify the boundaries.
2. Develop an appropriate concept model. The dimensions, governing equations, and numerical methods (e.g., finite element method, FEM) are decided based on the goals to be achieved and the hydrodynamic characteristics of the target water body.
3. Create the grid or mesh and define the boundary conditions.
4. Collect data (bathymetry, flow rate, water surface elevation, concentrations of contaminants, etc.) required for the model input, verification, and calibration.
5. Run the model.
6. Calibrate the model using the observed data.
7. Apply the model to simulate a real world scenario or solve a practical problem.

Based on aforementioned theory and principles, a stratified 3D model was used to investigate the circulation and *E. coli* transport in the nearshore region of Lake Michigan. The modeling results show that stratified phenomenon exists in the near region, and a 3D model is necessary. A 2D depth-averaged water quality model was developed to estimate the fate and transport of four contaminants in the San Joaquin River (SJR) of California. These models can be effectively used for inland surface water restoration and management.

Author details

Lubo Liu

Address all correspondence to: llubo@csufresno.edu

Department of Civil and Geomatics Engineering, Lyles College of Engineering, California State University Fresno, USA

References

[1] Stamou A, Polydera A, Papadonikolaki G, Martinez-Capel F, Munoz-Mas R, Papadaki C, Zogaris S, Bui MD, Rutschmann P, Dimitriou E. Determination of environmental flows in rivers using an integrated hydrological-hydrodynamic-habitat modelling approach. Journal of Environmental Management. 2018;**209**:273-285

[2] Lee I, Hwang H, Lee J, Yu N, Yun J, Kim H. Modeling approach to evaluation of environmental impacts on river water quality: A case study with Galing River, Kuantan, Pahang, Malaysia. Ecological Modelling. 2017;**353**:167-173

[3] Kim J, Lee T, Seo D. Algal bloom prediction of the lower Han River, Korea using the EFDC hydrodynamic and water quality model. Ecological Modelling. 2017;**366**:27-36

[4] Shakibaeinia A, Kashyap S, Dibike YB, Prowse TD. An integrated numerical framework for water quality modelling in cold-region rivers: A case of the lower Athabasca River. Science Total Environment. 2016;**569-570**:634-646

[5] Tang C, Yi Y, Yang Z, Zhang S, Liu H. Effects of ecological flow release patterns on water quality and ecological restoration of a large shallow lake. Journal of Cleaner Production. 2018;**174**:577-590

[6] Khadr M, Elshemy M. Data-driven modeling for water quality prediction case study: The drains system associated with Manzala Lake, Egypt. Ain Shams Engineering Journal. 2017;**8**(4):549-557

[7] Qi H, Lu J, Chen X, Sauvage S, Sanchez-Perez JM. Water age prediction and its potential impacts on water quality using a hydrodynamic model for Poyang Lake, China. Environmental Science and Pollution Research International. 2016;**23**(13):13327-13341

[8] Liang S, Jia H, Xu C, Xu T, Melching C. A Bayesian approach for evaluation of the effect of water quality model parameter uncertainty on TMDLs: A case study of Miyun reservoir. Science Total Environment. 2016;**560-561**:44-54

[9] Elshemy M, Khadr M, Atta Y, Ahmed A. Hydrodynamic and water quality modeling of Lake Manzala (Egypt) under data scarcity. Environmental Earth Sciences. 2016;**75**(19)

[10] Donia N, Bahgat M. Water quality management for Lake Mariout. Ain Shams Engineering Journal. 2016;**7**(2):527-541

[11] Xu C, Zhang J, Bi X, Xu Z, He Y, Gin KY. Developing an integrated 3D-hydrodynamic and emerging contaminant model for assessing water quality in a Yangtze estuary reservoir. Chemosphere. 2017;**188**:218-230

[12] Alosairi Y, Pokavanich T, Alsulaiman N. Three-dimensional hydrodynamic modelling study of reverse estuarine circulation: Kuwait Bay. Marine Pollution Bulletin. 2018;**127**: 82-96

[13] Silva Dos Santos E, Pinheiro Lopes PP, da Silva Pereira HH, de Oliveira Nascimento O, Rennie CD, da Silveira Lobo O'Reilly Sternberg L, and Cavalcanti da Cunha A, The impact of channel capture on estuarine hydro-morphodynamics and water quality in the Amazon delta. Science Total Environment, 2017;**624**:887-899

[14] Mali M, Malcangio D, Dell' Anna MM, Damiani L, Mastrorilli P. Influence of hydrodynamic features in the transport and fate of hazard contaminants within touristic ports. Case study: Torre a Mare (Italy). Heliyon. 2018;**4**. DOI: 10.1016/j.heliyon.2017.e00494

[15] Malcangio D, Petrillo AF. Modeling of brine outfall at the planning stage of desalination plants. Desalination. 2010;**254**(1–3):114-125

[16] Ji ZG. Hydrodynamics and Water Quality - Modeling Rivers, Lakes, and Estuaries. 1st ed. Hoboken, New Jersey: John Wiley & Sons, Inc.; 2007. 676 p

[17] Gill AE. Atmosphere-Ocean Dynamics. New York: Academic Press; 1982. 662 p

[18] Cole TM, Buchak EM. CE_QUAL-W2: A Two-Dimensional, Laterally Averaged, Hydrodynamic and Water Quality Model, Version 2. Vicksburg, MS: Technical Report El-95-X. US Army Corps of Engineers, Waterways Experiment Station; 1995

[19] Ford DE, Johnson MC. An Assessment of Reservoir Mixing Processes. Vicksburg, MS: Technical report, E-86-7: US Army Engineer Waterways Experiment Station; 1986

[20] Wu WM. Computational River Dynamics. London, UK: Taylor & Francis; 2008. 494 p

[21] Liu L, Phanikumar MS, Molloy SL, Whitman RL, Shiverly DA, Nevers MB, Schwab DJ, Rose JB. Modeling the transport and inactivation of *E. coli* and enterococci in the near-shore region of Lake Michigan. Environmental Science & Technology. 2006;**40**:5022-5028

[22] Smagorinsky J. General circulation experiments with the primitive equationsI. The basic experiment. Monthly Weather Review. 1963;**91**:99-164

[23] King IP. User Guide of RMA10-a Finite Element Model for Three-Dimensional Density Stratified Flow; User Guide of RMA11-a three Dimensional Finite Element Model for Water Quality in Estuaries and Stream. 2004

[24] Phillips NA. A coordinate system having some special advantage for numerical forecasting. Journal of Meteorology. 1957;**14**:184-185

[25] Mellor GL, Yamada T. Development of a turbulence closure model for geophysical fluid problems. Reviews of Geophysics and Space Physics. 1982;**20**(4):851-875

[26] Liu L, Fu XD, Wang GQ. Simulation of wind-driven circulation and temperature in the near-shore region of southern Lake Michigan by using a channelized model. Journal of Hydrodynamics. 2013;**25**(1):99-111

[27] Xia XS, Miller DH. The stratification analysis of sediment data for Lake Michigan. Journal of Data Science. 2011;**9**:181-203

[28] Liu L, Ramirez J. Assessment of spring Chinook salmon habitat suitability in the San Joaquin River using a 2-D depth-averaged model. International Journal of Water Sciences. 2013. DOI: 10.5772/57437

IntechOpen

IntechOpen